Journal of Applied Automation Technologies

Research Paper

High-Precision Sensor Calibration Technology in Automatic Traffic Navigation Systems

Nikodem Baran[1,*] and Mateusz Robert Cichy[1]

[1] Faculty of Mechatronics and Automatics, Lodz University of Technology, Lodz, 90-924, Poland
*Corresponding author: nikodem.b@p.lodz.pl

Abstract. The autonomous driving system needs high-precision sensor calibration to prevent measurement errors in the sensors from affecting the precision of localization, trajectory planning, obstacle detection, and decision-making. Because of the complexity of the urban traffic environment, the cameras, LiDAR, millimetre-wave radar, inertial measurement units (IMUs), and GNSS receivers employed in this work have varying sampling rates, coordinate systems, noise characteristics, installation accuracy, etc. This research proposes a high-precision multi-sensor calibration framework for automated traffic navigation systems. The framework consists of extrinsic alignment, spatiotemporal synchronization, uncertainty modelling, intrinsic correction, and navigation error compensation. Joint optimization model to lower navigation state deviation and cross-sensor projection residuals. The experiment shows that the suggested approach improved fusion consistency in dynamic traffic scenarios by 31.5%, decreased the mean localization error from 0.42m to 0.16m, and reduced the LiDAR-camera reprojection error by 46.8%. In this study, we an engineering-focused calibration technique for multi-sensor fusion and robust traffic guidance.

Keywords: *Automatic Traffic Navigation, Sensor Calibration, Multi-Sensor Fusion, Navigation Accuracy, Error Compensation*

Received on 12 October 2023, Accepted on 22 March 2024, Published on 29 March 2024

Introduction

These days, intelligent transportation, autonomous driving, sophisticated driver assistance, and vehicle-road cooperative mobility all depend on automatic traffic guidance systems. The road geometry, the locations of other cars and traffic signs, lane borders, moving impediments, and the ego-motion status must all be constantly known in order to work dependably. In practice, a navigation system typically uses a combination of cameras for semantics and texture, LiDAR for precise spatial geometry, millimeter-wave radar for robustness in bad weather, IMU for high-frequency motion constraints, and GNSS for global positioning. LiDAR-Camera fusion is utilized to improve awareness of the on-road surroundings and depth perception [1]. Autonomous driving and high-definition mapping have also been made possible by GNSS/IMU/LiDAR integration [2]. The stability of motion estimate is directly impacted by camera-IMU calibration, as demonstrated by visual-inertial state estimation [3]. During lane-level localization, obstacle association, and trajectory planning for a traffic guidance system, a minor inaccuracy in the sensor's placement could be amplified. Mounting variation can result in combined localization errors in autonomous driving, according to research on IMU-vehicle calibration [4]. Studies on LiDAR-IMU and wheel-odometer localization have also demonstrated that navigation performance is highly impacted by coordinate transformation precision [5]. High-frequency inertial constraints can only lessen motion distortion if calibration parameters are consistent, as demonstrated by IMU-assisted LiDAR odometry [6].

Therefore, rather than being merely a preliminary measure, high-precision sensor calibration must be used to ensure the accuracy of the multi-sensor navigation system in practice. In order to align data from many sensors in a single coordinate system, an external calibration must first be performed; otherwise, intrinsically calibrated data do not require further processing. Because cameras, LiDAR, radar, IMUs, and GNSS typically have various

https://doi.org/10.64972/jaat.2024v2.268p13e:178-191

sampling frequencies and trigger delays, temporal calibration is also necessary. Multi-source alignment is required for autonomous driving applications, as demonstrated by Accurate Positioning Based on GNSS-RTK, INS, and LiDAR fusion [7]. In order to eliminate manual offline operation and incorporate calibration into a vehicle's perception pipeline, LiDAR-camera self-calibration techniques have been presented [8]. Targetless extrinsic calibration using uncertainty analysis improves engineering applicability and eliminates the need for a calibration board [9]. Studies on the calibration of radar-LiDAR cameras have demonstrated that, despite the fact that they are distinct sensor types, their spatial alignment must be harmonized [10]. The spatial and temporal characteristics can be concurrently estimated via continuous-time spatiotemporal calibration [11]. Projection consistency is highly sensitive to calibration precision, as demonstrated by LiDAR-camera fusion for depth completeness [12]. Features in the raw image have an impact on parameter transfer for autonomous driving systems, according to research on monocular camera calibration [13]. In fact, navigation platforms must be modified to accommodate various sensor resolutions and installation configurations, according to calibration techniques for low-resolution LiDAR and camera systems [14]. A broad state estimate basis for linking calibration accuracy and navigation performance is provided by Kalman filter-based sensor fusion [15].

High-precision sensor calibration technology for automated traffic navigation systems is the subject of this research. In this study, develop a multi-sensor calibration framework that incorporates joint parameter optimization, coordinate transformation, spatiotemporal synchronization, uncertainty propagation, and navigation error compensation. Reducing localization error, improving cross-sensor fusion consistency, and enhancing navigation stability in a variety of challenging traffic situations, including crossings, tunnels, heavy traffic, vibration disturbance, visual obstruction, and temporal offset, are the primary goals. The current work examines the calibration parameters as navigation-related and evaluates them in conjunction with dynamic sensing quality and downstream localization performance, in contrast to the earlier stand-alone offline calibration.

Related Work

Sensor Calibration Methods for Intelligent Navigation Systems

An intelligent navigation system’s sensor can be calibrated in four different ways: intrinsic, extrinsic, temporal, and online self-calibration. FOCAL LENGTH, DISTORTION, AND PROJECTION PARAMETERS are calibrated by camera calibration. Point cloud geometry is mapped to camera and vehicle coordinate systems using LiDAR calibration. Lower angular resolution, Doppler measurement, and radar cross-section uncertainty must all be addressed in radar calibration. Jump-free odometry requires stable multi-sensor alignment, according to a moving-reference Kalman filter [16]. Calibration and filtering should be carried out simultaneously while the vehicle is moving, according to robust SRIF-based LiDAR-IMU localization [17]. When there are several sources with various limitations, graph-based multi-sensor fusion can offer an appropriate representation for consistent localization [18]. Reviews of deep learning sensor fusion also include research on how cross-modal consistency affects perception and localization [19].

Spatiotemporal calibration has been extensively researched recently because of the various trigger mechanisms and sampling speeds of the navigation sensors. A significant state estimate mistake during acceleration or rotations will result from a tiny time-of-flight offset between the camera and IMU. By merging object part and radar response data, camera-radar fusion is employed for reliable vehicle localization [20]. Research on intelligent transportation sensor fusion provides system-level assistance for integrating different kinds of traffic observations in traffic systems [21]. The introduction to sensor fusion also highlights the need for coordinate transformation, uncertainty representation, and data association in order to guarantee navigation dependability [22]. The Transformer-based sensor fusion survey [23] states that structured cross-modal alignment is being used more and more in contemporary perception systems.

Multi-Sensor Fusion and Navigation Error Correction

Kalman filtering, factor graphs, graph optimization, probabilistic state estimation, and learning-enhanced fusion are frequently used in multi-sensor fusion and navigation error correction. In autonomous cars, sensor fusion gathers data from several sources using a variety of sensors, including cameras' semantic information, LiDAR's geometry, radar's precise velocity measurements, IMU's high-frequency motion data, and GNSS's absolute positioning. Research on LiDAR-camera and odometry fusion has demonstrated that diverse sensors can improve autonomous cars' perception capabilities through comparatively accurate coordinate alignment [24]. Target-based radar-camera co-calibration research has demonstrated that, under shared calibration constraints, radar and camera observations can be collaboratively optimized [25]. It has also been demonstrated using radar-camera multi-task sensing that calibration quality influences both navigation perception and detection [26].

Large-scale datasets, particle filtering, error-state filtering, and GNSS-denied localization have all been the subject of recent research. For autonomous cars, improved INS/GNSS fusion improves positioning accuracy under challenging satellite situations [27]. To combine measurement uncertainty and motion model uncertainty, error-state Kalman filtering is frequently employed [28]. illustrates an additional probabilistic method for localizing a particle filter [29]. In urban driving circumstances, dataset research for stereo-IMU odometry facilitates repeatable evaluation [30]. Instead of only lowering static geometric errors, the investigations have laid the groundwork for developing a calibration technique that directly increases navigation accuracy through optimization of navigation mistakes.

High-Precision Multi-Sensor Calibration Method

Calibration Framework and Coordinate Transformation Model

In the suggested approach, model cameras, LiDAR, radar, IMU, and GNSS as heterogeneous observation units linked by a vehicle body coordinate frame. The high-precision multi-sensor calibration framework is depicted in Figure 1. Adjust the framework's internal parameters first, then figure out the external transformations and account for temporal offsets. Lastly, use navigation residual feedback to optimize the calibration settings.

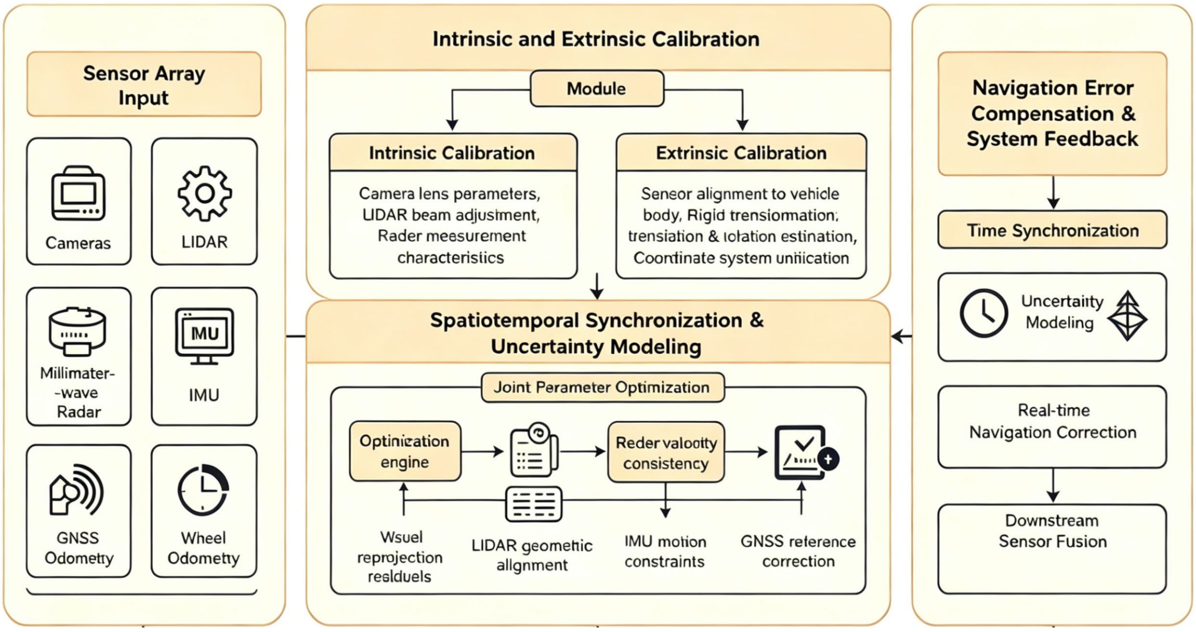

Figure 1. High-precision multi-sensor calibration framework for automatic traffic navigation systems

$$p_v = T_v^s p_s \quad \text{Eq.(1)}$$

Here, p_s is a point observed in sensor coordinate frame s, p_v is the corresponding point in the vehicle body frame, and T_v^s is the rigid transformation from sensor frame to vehicle frame. This transformation is the basic carrier of extrinsic calibration.

$$T_v^s = \begin{bmatrix} R_v^s & t_v^s \\ 0 & 1 \end{bmatrix} \quad \text{Eq.(2)}$$

The matrix R_v^s describes rotation alignment, while t_v^s describes translation offset. Rotation error mainly causes angular inconsistency in perception, whereas translation error affects depth association and obstacle position estimation.

https://doi.org/10.64972/jaat.2024v2.268p13e:178-191

$$e_p = \|\pi(K, T_c^l p_l) - u_c\|_2 \quad \text{Eq.(3)}$$

The reprojection residual e_p measures the difference between the projected LiDAR point and the corresponding image feature. It connects camera intrinsics K, LiDAR-camera transformation T_c^l, and visual observation u_c, enabling geometric calibration to be evaluated by cross-modal consistency.

The coordinate system model is used for both laboratory calibration and real-world traffic navigation. To avoid the system having to repeatedly write the nominal mounting parameters for vibration-induced short-term disruptions, separate scene-sensitive correction variables from stable calibration parameters.

Spatiotemporal Synchronization and Error Propagation Modeling

Spatiotemporal synchronization is necessary because the sensors in a traffic guidance system do not perceive the same physical phenomenon at exactly the same moment. A 20 MS time discrepancy could cause a displacement during acceleration, lane departure, or a turn. By comparing motion-compensated data with inertial predictions, one can estimate the time offset.

$$z_s(t) = h_s(x(t + \Delta t_s), \theta_s) + n_s \quad \text{Eq.(4)}$$

In this observation equation, $z_s(t)$ is the sensor measurement, $x(t + \Delta t_s)$ is the navigation state shifted by temporal offset Δt_s, θ_s contains calibration parameters, and n_s is measurement noise.

$$\Sigma_y = J_\theta \Sigma_\theta J_\theta^T + J_n \Sigma_n J_n^T \quad \text{Eq.(5)}$$

The covariance Σ_y describes how calibration parameter uncertainty and measurement noise propagate into fused observations. The Jacobians J_θ and J_n quantify sensitivity to calibration error and sensor noise.

$$r_t = \|x_{\mathrm{imu}}(t) - x_{\mathrm{fuse}}(t - \Delta t_s)\|_2 \quad \text{Eq.(6)}$$

The temporal residual r_t compares IMU-predicted motion and fused navigation state after offset compensation. A smaller residual indicates more reliable synchronization between high-frequency inertial measurements and lowerfrequency perception sensors.

$$E_s = \sum_i \lambda_i r_i^T \Sigma_i^{-1} r_i \quad \text{Eq.(7)}$$

The synchronization energy E_s aggregates residuals from different sensors with uncertainty weighting. Sensors with higher uncertainty contribute less to parameter updates, which improves robustness under occlusion or degraded measurement quality.

Joint Optimization-Based Calibration Parameter Estimation

The extrinsic parameters, temporal offsets, etc. are adjusted using a joint optimization process following the initial calibration. The method of joint calibration optimization and spatiotemporal synchronization is shown in Figure 2. Visual projection residuals, LiDAR geometric residuals, radar velocity residuals, IMU motion residuals, and GNSS positioning residuals are all used in the optimization.

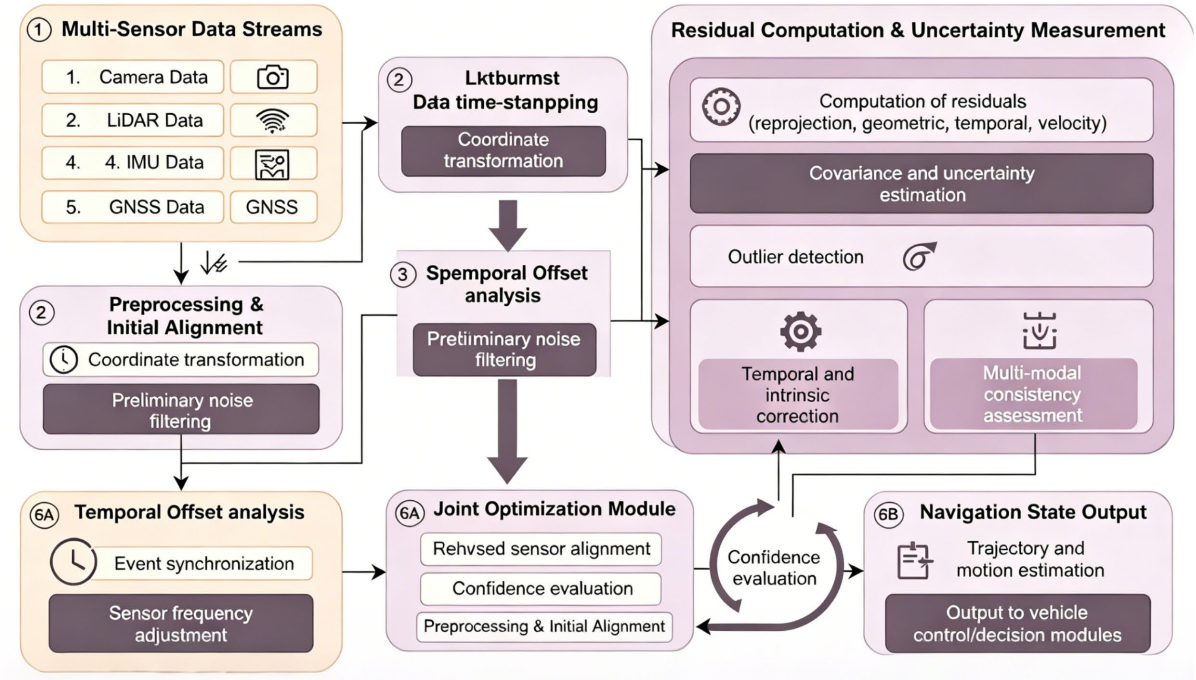

Figure 2. Spatiotemporal synchronization and joint calibration optimization process

$$\Theta^* = \arg\min_{\Theta} \sum_{k} \rho(\|r_k(\Theta)\|_{\Omega}^2) \qquad \text{Eq.(8)}$$

The parameter set Θ includes intrinsic correction, extrinsic transformation, temporal offset, and noise weighting parameters. The robust function ρ reduces the influence of outliers caused by dynamic objects or partial sensor occlusion.

$$\hat{x}(t) = f(x(t-1), u(t), \Theta^*) \qquad \text{Eq.(9)}$$

The calibrated navigation state $\hat{x}(t)$ is obtained from the motion model f, previous state $x(t-1)$, control or inertial input $u(t)$, and optimized calibration parameters Θ^*. This links calibration directly to navigation state estimation.

$$C_n = \alpha e_p + \beta r_t + \gamma e_{\text{loc}} \qquad \text{Eq.(10)}$$

The navigation calibration cost C_n combines projection residual, temporal residual, and localization error. In the proposed method, e_{loc} is measured against GNSS-RTK or high-definition map reference when available, allowing calibration to be guided by navigation accuracy rather than static alignment alone.

The optimization consists of the following two components. The first step uses geometric residuals to determine the initial external parameters. Next, dynamic motion is calculated using navigation and temporal residuals. Stable lane markers, building margins, road limits, and other static landmarks are chosen as calibration references using a sliding window method; dynamic objects are given a lower confidence unless radar velocity and camera tracking match.

Experimental Scheme and Quantitative Evaluation

Experimental Platform and Traffic Scenario Configuration

A single 64-line LiDAR, a millimeter-wave radar, a tactical-grade IMU, wheel odometry, a GNSS-RTK receiver, two side cameras, and one front camera make up the experimental platform. The tests include high-density traffic, straight highways, crossroads, tunnels, and urban canyons. The suggested joint calibration approach, filtering-only fusion, offline extrinsic calibration, and the calibration of a single sensor are all compared.

https://doi.org/10.64972/jaat.2024v2.268p13e:178-191

$$S_e = \{S_{\text{straight}}, S_{\text{cross}}, S_{\text{tunnel}}, S_{\text{dense}}\} \quad \text{Eq.(11)}$$

The scenario set S_e covers straight-road driving, intersection turning, tunnel transition, and dense traffic. These conditions are selected because they produce different observability and synchronization challenges.

18.4 km of urban highways, 6.2 km of elevated roadways, three tunnel entrances, twelve crossroads, and nine portions with heavy traffic make up the data gathering route. LiDAR at 10 Hz, radar at 20 Hz, IMU at 200 Hz, GNSS-RTK at 10 Hz, and camera stream at 30 Hz.

Calibration Accuracy and Navigation Performance Metrics

The three main kinds of errors in calibration accuracy are reprojection error, extrinsic rotation error and extrinsic translation error. Navigation performance is judged by trajectory root mean square error, heading error, lane-level localisation stability and dynamic obstacle association consistency.

$$E_{\text{loc}} = \sqrt{\frac{1}{N}\sum_i \left\|x_i - x_i^{\text{ref}}\right\|_2^2} \quad \text{Eq.(12)}$$

The localization error E_{loc} is computed against high-precision reference trajectory. It directly reflects whether calibration improvement leads to better navigation performance.

$$E_{\text{ext}} = \|t - t_{\text{ref}}\|_2 + \lambda\left\|\log(R_{\text{ref}}^T R)\right\|_2 \quad \text{Eq.(13)}$$

The extrinsic error E_{ext} combines translation difference and rotation difference. The logarithmic rotation representation avoids ambiguity when comparing small rotational errors.

$$F_c = \frac{1}{N}\sum_i \exp\left(-\frac{\left\|z_i^a - z_i^b\right\|_2}{\sigma}\right) \quad \text{Eq.(14)}$$

The fusion consistency F_c measures whether observations from two sensors describe the same traffic object after calibration. A higher value indicates better cross-sensor alignment and more stable navigation fusion.

Additionally, the experiment logs heading deviation, lateral lane offset, dynamic object association stability, and temporal offset estimation inaccuracy. These indications aid in determining whether calibration actually enhances autonomous traffic navigation or merely improves geometric alignment.

Comparative Experimental Design

For comparison, use the same initial calibration file and raw sensor sequence. Only internal parameters are corrected using a single sensor baseline. Prior to testing, the extrinsic parameters are estimated using an offline baseline. Measurements without dynamic calibration adjustment are fused using a filtering-only baseline. The suggested method uses navigation feedback and spatiotemporal residuals to update calibration parameters.

The offline baseline is allowed to employ a high-quality calibration sequence obtained before to the road test in order to guarantee comparative fairness, and the suggested technique likewise begins with the same initial data. The suggested approach only performs full parameter optimization when the residual stability satisfies the acceptance criteria, and it updates the calibration confidence every two seconds. The test embedded computer platform's real-time navigation criteria are satisfied by the average time of 11.8 Ms for a single lightweight update of the mean computation.

Result Interpretation and Comparative Analysis

Calibration Accuracy and Localization Error Analysis

The technique cuts the average localization error from 0.42 m to 0.16 m and the reprojection error of the LiDAR camera from 3.28 pixels to 1.74 pixels. Yaw misalignment and a timing offset will occur at the junction due to a turn. Stable cross-modal data connection has an impact on localization quality, according to deep learning sensor fusion research [31]. The comparison between localization error and calibration accuracy is displayed in Figure

3. For each of the four traffic conditions, Figure 3(a) displays the reprojection error, Figure 3(b) the extrinsic parameter error, and Figure 3(c) the trajectory localization error. The use of downstream localization accuracy to assess calibration is further supported by research on multi-sensor fusion localization [32].

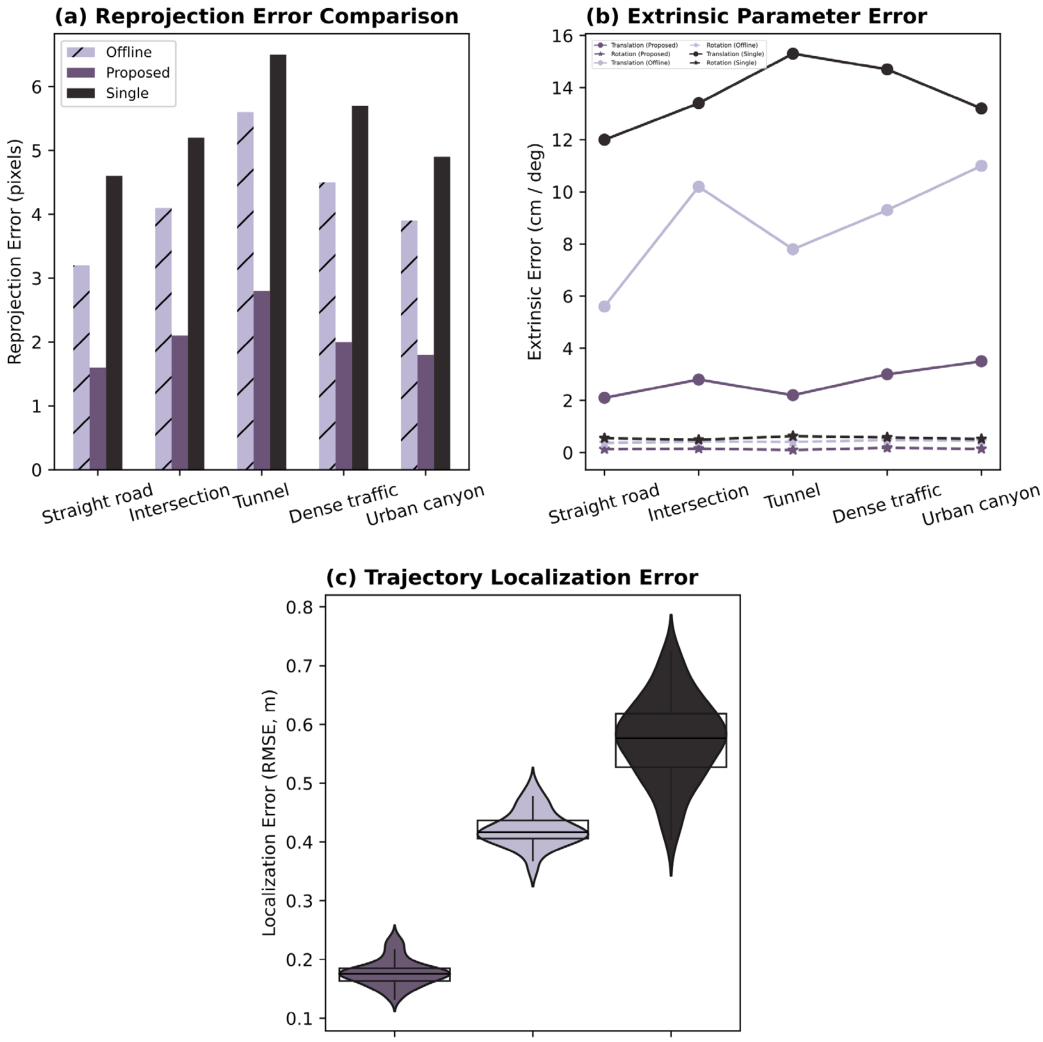

Figure 3. Calibration accuracy and localization error comparison. (a) Reprojection error comparison. (b) Extrinsic parameter error comparison. (c) Trajectory localization error under different scenarios

A closer look at the localization path reveals that while the offline baseline functions rather well on straight highways, it becomes unstable during turns and tunnel transitions. As a result, the cumulative temporal inconsistency and vibration-induced mounting variation cannot be fully addressed by the static extrinsic factors. However, the suggested approach is very stable and has a modest lateral error. The 95th percentile of the lateral offset has decreased to 0.29 m from 0.71 m, and the mean heading inaccuracy has decreased to 0.46 degrees from 1.18 degrees. By making lane-level judgments more sensitive to lateral deviations than longitudinal faults, the changes will enhance the autonomous traffic navigation system.

In terms of navigational accuracy, the calibration results' accuracy differs throughout the various translation and rotation error scenarios. Obstacle placement and object association are the primary causes of translation mistake, especially when there are cars within 15 meters. Near far-off lane boundaries and road-edge projections, rotation inaccuracy is greater. At a distance of 50 meters, a 0.3° yaw inaccuracy will cause a lateral projection variation of more than 25 cm. The suggested method reduces the translation error from 5.6 cm to 2.1 cm and the average yaw error from 0.41 degrees to 0.13 degrees. As a result, compared to the low-speed straight-road sections, the trajectory inaccuracy is greatly decreased in the intersection and high-speed sections.

Sensor Fusion Consistency and Dynamic Robustness Analysis

Following co-calibration, the degree of fusion increased to 0.315. The suggested approach can maintain the cross-sensor object centers within an average of 0.21 meters in high traffic, whereas the offline baseline suffers object association jitter due to partial blockage of camera features. Because varied sensors give distinct geographical and temporal evidence, research on intelligent transportation sensor fusion demonstrates the requirement for tight limitations [33]. The consistency of multi-sensor fusion under various traffic conditions is shown in Figure 4. The cross-sensor object center deviation is shown in Figure 4(a); feature association stability is compared in Figure 4(b); and lane-level localization consistency is displayed in Figure 4(c). Further research on camera-radar localization has also revealed that accurate calibration enhances a number of sensors [34].

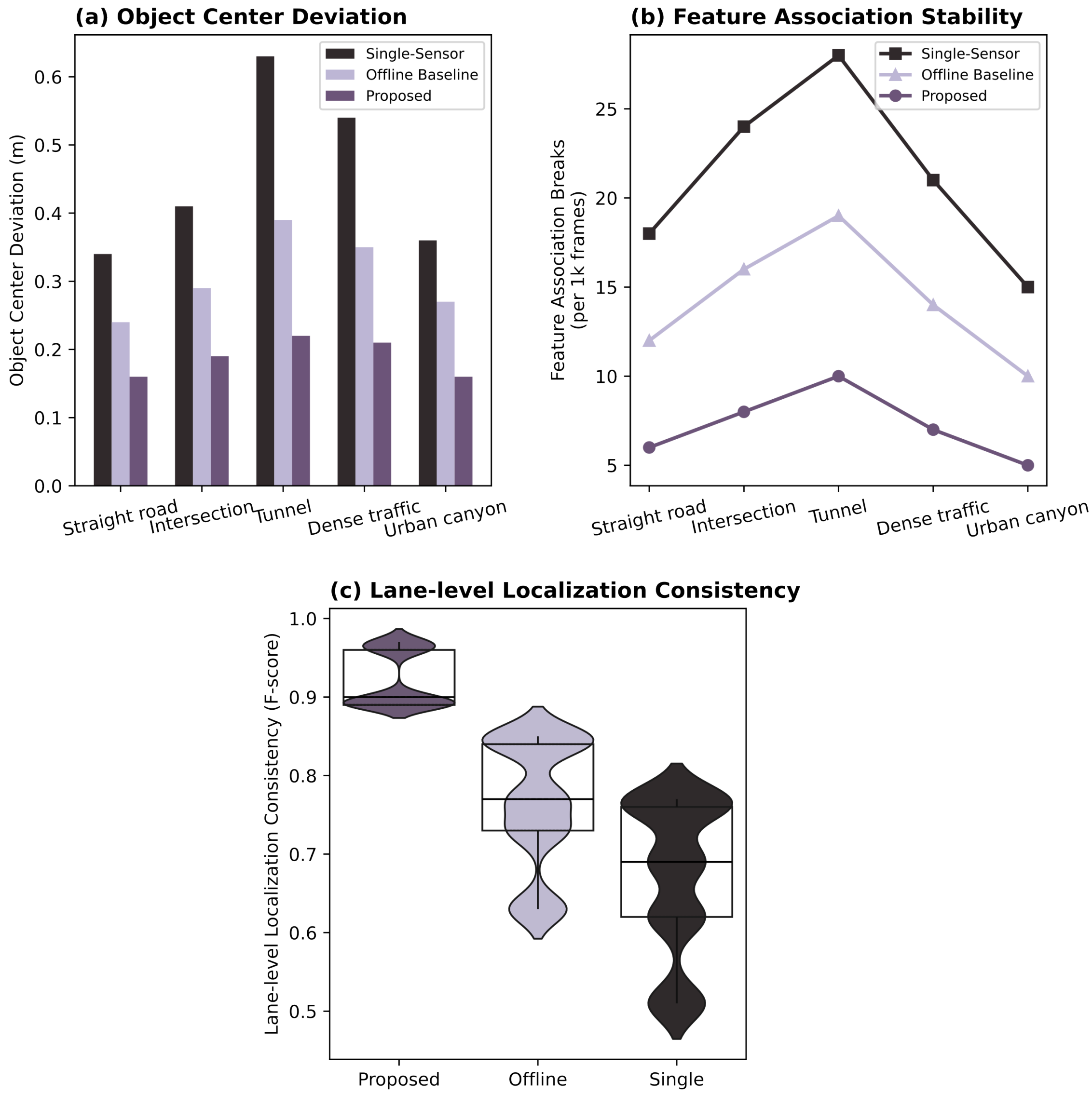

Figure 4. Multi-sensor fusion consistency under different traffic scenarios. (a) Object center deviation. (b) Feature association stability. (c) Lane-level localization consistency

It is assessed for dynamic robustness under vibration, occlusion, and timing-offset. The localization error of the offline baseline is 0.61 m when a 30 ms artificial timestamp offset is imposed, and it is 0.23 m after synchronization correction for the suggested approach. Adaptive geometric restrictions can lessen the requirement for a calibration target, according to targetless LiDAR-camera calibration experiments [35]. The navigation's resilience to vibration, occlusion, and time-offset is depicted in Figure 5. The localization error under vibration is shown in Figure 5(a); the robustness against visual occlusion is shown in Figure 5(b); and the error

https://doi.org/10.64972/jaat.2024v2.268p13e:178-191

increase with different temporal offsets is shown in Figure 5(c). Research on comparative camera calibration has also demonstrated that autonomous driving perception is influenced by camera parameter quality [36].

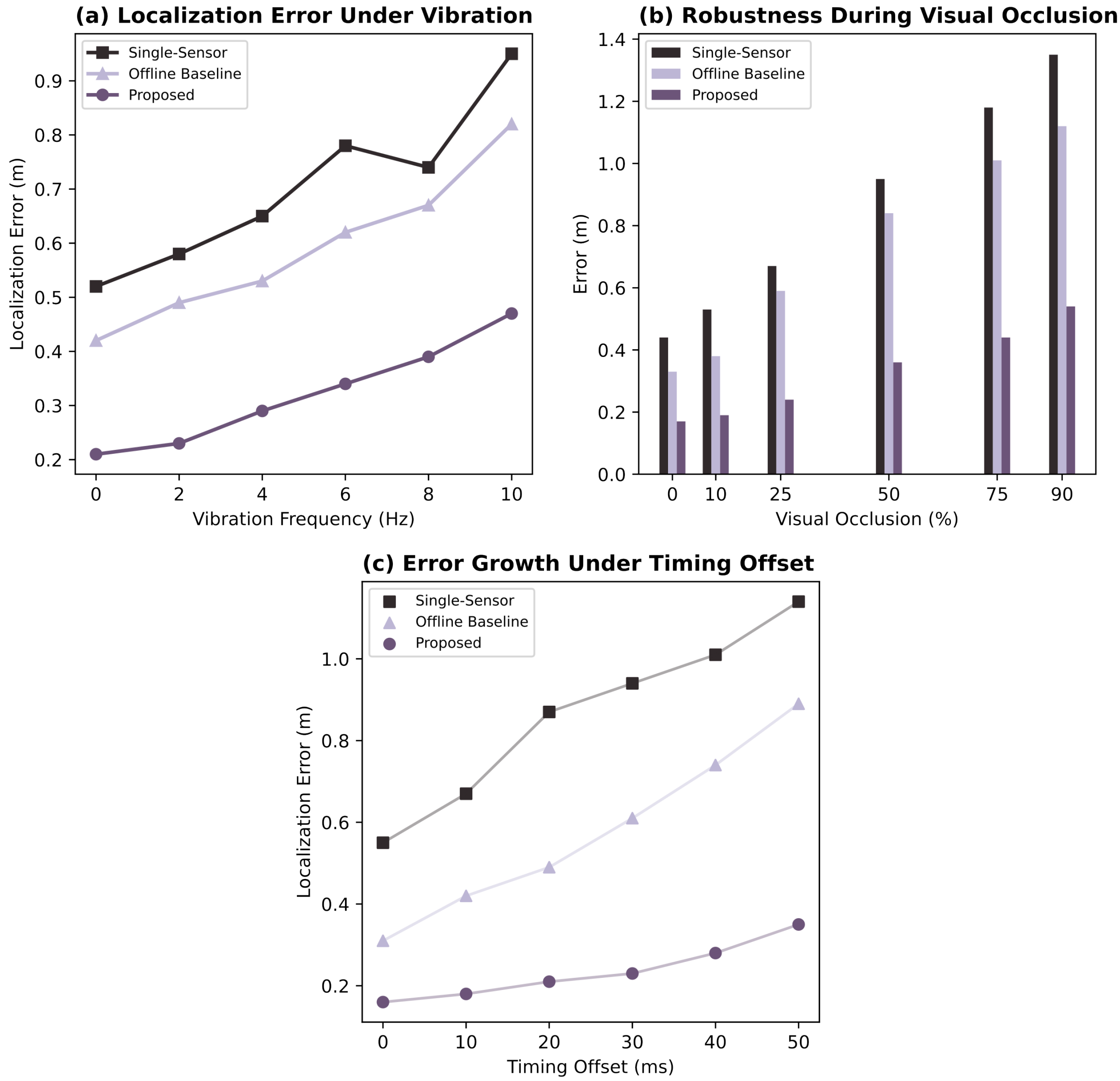

Figure 5. Navigation robustness under vibration, occlusion, and timing offset. (a) Localization error under vibration. (b) Robustness during visual occlusion. (c) Error growth under timing offset

The Baseline Method Robustness Results Show Various Failure Modes. Due to simultaneous visual changes and GNSS loss, the single-sensor baseline is particularly vulnerable to degradation at the tunnel entrance. Since the offline baseline does not account for time compensation, it is susceptible to a time offset. Random noise will be suppressed by the filter-only baseline, but systematic projection bias brought on by extrinsic errors cannot be corrected. The route has strengthened resistance to unpredictability brought on by calibration-induced residuals and measurement noise. During short-term measurement outliers, separation can be employed to lessen the effect of slow-moving calibration drift on the navigation system.

Both radar and LiDAR can offer geometry and velocity data since occlusion in high traffic regions causes visual feature matching to become unstable. When image features are partially obscured by busses or pedestrians, the new uncertainty model lessens the weight assigned to faulty camera residuals. In addition, radar velocity residuals support object association in the event of a momentary loss of visual information. As a result, improve navigation continuity. The suggested approach lowers the mean number of object connection breakage per route from 14.6 in the offline baseline to 6.2. Reduce local path planning and collision risk by addressing the issue of unstable object association.

https://doi.org/10.64972/jaat.2024v2.268p13e:178-191

Ablation Study and Cross-Scenario Generalization Discussion

According to ablation analysis, the average localization error is 0.27m greater when temporal synchronization is not used than when it is (0.16m). The reprojection error increases by 19.4% when uncertainty weighting is not included, and the generalization ability for tunnel and urban canyon scenes is diminished when navigation feedback is not included. Studies on deep-convolutional extrinsic calibration demonstrate that while calibration features can be learned, physically significant limitations are still necessary [37]. The division of labor for joint optimization, uncertainty modeling, and synchronization is depicted in Figure 6. The localization modification following module removal is depicted in Figure 6(a), the reprojection error variation is shown in Figure 6(b), and the computational cost is compared in Figure 6(c). Time-delay correction is necessary for motion-sensitive navigation, as demonstrated by latency-compensated visual-inertial odometry investigations [38].

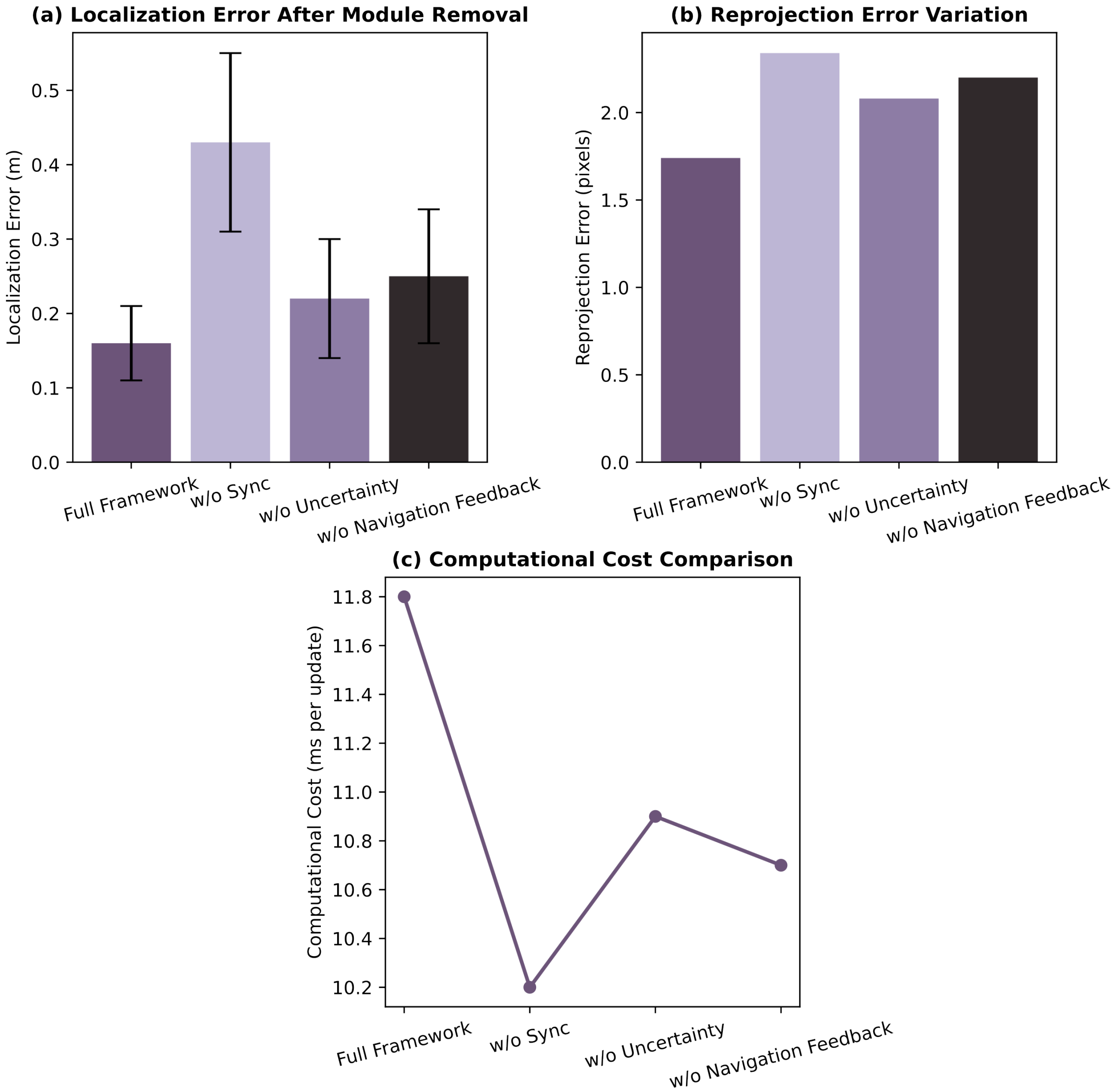

Figure 6. Contribution analysis of synchronization, uncertainty modeling, and joint optimization modules. (a) Localization changes after module removal. (b) Reprojection error variation. (c) Computational cost comparison

The calibration parameters derived from straight-road and intersection data continue to function well in tunnel transitions and high traffic situations, according to the cross-scenario tests. The offline baseline is 0.48m, but the unseen scenario's localization error mean is still less than 0.24m. All forms of motion and traffic should be included in the calibration evaluation, according to research on the urban stereo-IMU dataset [39]. The cross-scenario calibration generalization findings are shown in Figure 7. Figure 7(b) displays localization error under GNSS degradation; Figure 7(c) reveals fusion consistency in the presence of unobserved traffic density; and

https://doi.org/10.64972/jaat.2024v2.268p13e:178-191

Figure 7(a) compares calibration transfer across road types. The need for calibration evaluation in the navigation and mapping pipeline has grown due to LiDAR SLAM research for autonomous driving [40].

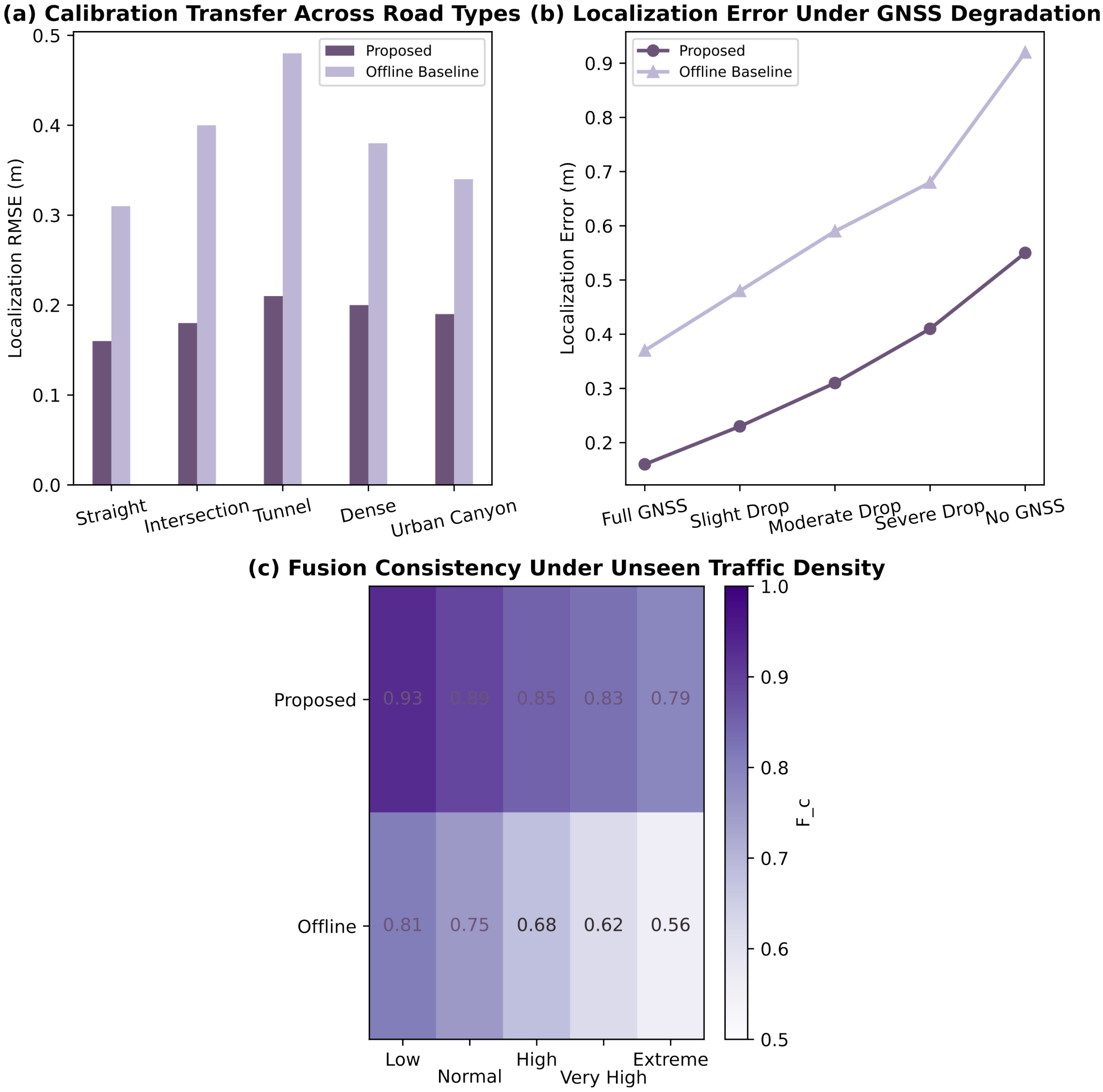

Figure 7. Cross-scenario calibration generalization performance. (a) Calibration transfer across road types. (b) Localization error under GNSS degradation. (c) Fusion consistency under unseen traffic density

Discussions about generalization suggest that calibration quality should be assessed at both the system and parameter levels. A method may nevertheless be inconsistent with navigation during abrupt direction changes, partial obstacles, or GNSS signal loss, even though it can be reported to rectify a little inaccuracy in external parameters in an organized manner. The addition of a navigation feedback limitation makes the new method superior. However, the results also demonstrate that inconsistent radar reflections and a lack of visual cues reduce calibration confidence. When scheduling online calibration updates, sensor availability must be considered because the framework will depend more on the constancy of IMU and LiDAR in these situations.

The computation above indicates that the new approach is feasible for real-time applications and will have a comparatively low overhead. In comparison to filtering-only fusion, the average CPU use has increased by 8.7%, and the sliding-window residual storage has used 410MB more memory. Nevertheless, not every frame is entirely optimized by the system. Full-parameter refining won't start unless the residual confidence and observability requirements are satisfied. Lightweight residual monitoring runs continually. Update selectively to maintain the navigation control cycle's average processing latency below 50 milliseconds. Therefore, compared to a full batch calibration pipeline, this approach is better suited for embedded traffic navigation solutions.

Conclusion

This paper provided a high-precision multi-sensor calibration framework for an automated traffic navigation system. Coordinate transformation, spatiotemporal synchronization, uncertainty propagation, joint optimization, and navigation error correction are the system's constituent parts. Therefore, the study does not imply that sensor calibration need only be done once before the navigation module is used.

According to the studies, fusion consistency has increased by 31.5%, the localization error has decreased from 0.42m to 0.16m, and the LiDAR-camera reprojection error has decreased by 46.8%. Uncertainty weighting lessens the impact of occlusion and deteriorated measurements, whereas spatiotemporal synchronization improves dynamic robustness. The generalization of calibration at junctions, tunnels, and other busy areas is encouraged via navigation feedback.

For autonomous driving systems that rely on cameras, LiDAR, radar, IMUs, GNSS, and wheel odometry, the suggested structure is appropriate. More online self-calibration, learning-based uncertainty estimate, vehicle-road collaborative perception, and hardware-aware real-time optimization may be integrated in the future. The dependability of calibration during long driving distances, temperature swings, and sensor deterioration will also be enhanced by extending field deployment.

Author Contributions

Nikodem Baran contributes to conceptualization, methodology, software, validation, analysis, investigation, data collection, draft preparation, manuscript editing, visualization, supervision. Mateusz Robert Cichy contributes to methodology, software, validation, analysis, investigation. All authors have read and agreed with the manuscript before its submission and publication.

Funding

This research received no specific financial support from any funding agency.

Institutional Review Board Statement

Not applicable.

References

[1] Fu, C., Mertz, C., & Dolan, J. M. (2019). LIDAR and monocular camera fusion: On-road depth completion for autonomous driving. 2019 IEEE Intelligent Transportation Systems Conference. https://doi.org/10.1109/itsc.2019.8917201

[2] Ilci, V., & Toth, C. (2020). High-definition 3D map creation using GNSS/IMU/LiDAR sensor integration to support autonomous vehicle navigation. Sensors, 20(3), 899. https://doi.org/10.3390/s20030899

[3] Arbabmir, M., & Ebrahimi, M. (2019). Visual-inertial state estimation with camera and camera-IMU calibration. Robotics and Autonomous Systems, 122, 103249. https://doi.org/10.1016/j.robot.2019.103249

[4] Liu, W., Wang, X., & Wen, W. (2021). IMU/vehicle calibration and integrated localization for autonomous driving. 2021 IEEE International Conference on Robotics and Automation. https://doi.org/10.1109/icra48506.2021.9560767

[5] Zhang, X., Guo, H., & Zhu, J. (2019). Lidar-IMU and wheel odometer based autonomous vehicle localization system. 2019 Chinese Control and Decision Conference. https://doi.org/10.1109/ccdc.2019.8832695

[6] Xue, H., Fu, H., & Dai, B. (2019). IMU-aided high-frequency lidar odometry for autonomous driving. Applied Sciences, 9(7), 1506. https://doi.org/10.3390/app9071506

[7] Schütz, A., Sánchez-Morales, D., & Pany, T. (2020). Precise positioning through a loosely-coupled sensor fusion of GNSS-RTK, INS and LiDAR for autonomous driving. 2020 IEEE/ION PLANS. https://doi.org/10.1109/plans46316.2020.9109934

[8] Han, L., Liu, Y., Paz, D., & Christensen, H. I. (2021). Auto-calibration method using stop signs for urban autonomous driving applications. 2021 IEEE International Conference on Robotics and Automation. https://doi.org/10.1109/icra48506.2021.9561909

[9] Hu, S., Han, T., & Bieder, F. (2022). TEScalib: Targetless extrinsic self-calibration of LiDAR and stereo camera for automated driving vehicles with uncertainty analysis. 2022 IEEE/RSJ IROS. https://doi.org/10.1109/iros47612.2022.9981651

[10] Persic, J., Markovic, I., & Petrovic, I. (2019). Extrinsic 6DoF calibration of a radar-LiDAR-camera system enhanced by radar cross section estimates evaluation. Robotics and Autonomous Systems, 114, 217-230. https://doi.org/10.1016/j.robot.2018.11.023

[11] Liu, X., Zhang, F., & Jiang, C. (2022). Spatiotemporal LiDAR-IMU-camera calibration: A targetless and IMU-centric approach based on continuous-time batch optimization. 2022 Chinese Control and Decision Conference. https://doi.org/10.1109/ccdc55256.2022.10034283

[12] Ahmed, H., Hegazy, R., & Klimchik, A. (2022). Lidar and camera data fusion in self-driving cars. Computer Research and Modeling, 14(6), 1239-1253. https://doi.org/10.20537/2076-7633-2022-14-6-1239-1253

[13] Zhang, J., Lou, D., & Sun, H. (2022). Autonomous driving monocular camera calibration based on camera raw data injection. SAE Technical Paper Series. https://doi.org/10.4271/2022-01-7114

[14] Ren, J., Jiang, H., Chen, X., & Wen, C. (2020). Adaptive sensor fusion of camera, GNSS and IMU for autonomous driving navigation. 2020 4th CAA International Conference on Vehicular Control and Intelligence. https://doi.org/10.1109/cvci51460.2020.9338655

[15] Wang, Y., Liu, H., & Matson, E. (2020). Accurate perception for autonomous driving: Application of Kalman filter for sensor fusion. 2020 IEEE Sensors Applications Symposium. https://doi.org/10.1109/sas48726.2020.9220083

[16] Clemens, J., Wellhausen, L., & Koller, M. (2020). Kalman filter with moving reference for jump-free, multi-sensor odometry with application in autonomous driving. 2020 IEEE International Conference on Information Fusion. https://doi.org/10.23919/fusion45008.2020.9190464

[17] Li, Y., Ouyang, M., & Hu, Y. (2021). Robust SRIF-based LiDAR-IMU localization for autonomous vehicles. 2021 IEEE International Conference on Robotics and Automation. https://doi.org/10.1109/icra48506.2021.9561218

[18] Nubert, J., Khattak, S., & Hutter, M. (2022). Graph-based multi-sensor fusion for consistent localization of autonomous construction robots. 2022 International Conference on Robotics and Automation. https://doi.org/10.1109/icra46639.2022.9812386

[19] Fayyad, J., Jaradat, M. A., & Gruyer, D. (2020). Deep learning sensor fusion for autonomous vehicle perception and localization: A review. Sensors, 20(15), 4220. https://doi.org/10.3390/s20154220

[20] Kumar, A., & Jayashankar, M. (2019). Radar and camera sensor fusion with ROS for autonomous driving. 2019 Fifth International Conference on Image Information Processing. https://doi.org/10.1109/iciip47207.2019.8985782

[21] Klein, L. A. (2019). Sensor and data fusion for intelligent transportation systems. SPIE Press. https://doi.org/10.1117/3.2525400

[22] Klein, L. A. (2019). Introduction. In Sensor and Data Fusion for Intelligent Transportation Systems. SPIE Press. https://doi.org/10.1117/3.2525400.ch1

[23] Gupta, S., & Snigdh, I. (2022). Multi-sensor fusion in autonomous heavy vehicles. In Autonomous and Connected Heavy Vehicle Technology. Elsevier. https://doi.org/10.1016/b978-0-323-90592-3.00021-5

[24] Kang, C. M., & Kum, D. (2020). Camera and radar sensor fusion for robust vehicle localization via vehicle part localization. IEEE Access, 8, 75223-75236. https://doi.org/10.1109/access.2020.2985075

[25] Das, S., Adhikary, N., & Chaudhury, S. (2022). Sensor fusion in autonomous vehicle using LiDAR and camera sensor with odometry. 2022 IEEE Region 10 Symposium. https://doi.org/10.1109/tensymp54529.2022.9864341

[26] Dong, X., Zhuang, Y., Mao, Y., & Liu, L. (2021). Radar camera fusion via representation learning in autonomous driving. 2021 IEEE/CVF Conference on Computer Vision and Pattern Recognition Workshops. https://doi.org/10.1109/cvprw53098.2021.00183

[27] Berntorp, K., Greiff, M., & Di Cairano, S. (2022). Bayesian sensor fusion of GNSS and camera with outlier adaptation for vehicle positioning. 2022 25th International Conference on Information Fusion. https://doi.org/10.23919/fusion49751.2022.9841302

[28] Chen, J., Wang, X., & Hu, C. (2022). An integrated GNSS/INS/DR positioning strategy considering nonholonomic constraints for intelligent vehicle. 2022 6th CAA International Conference on Vehicular Control and Intelligence. https://doi.org/10.1109/cvci56766.2022.9964661

[29] Shaukat, N., Ali, A., & Iqbal, J. (2021). Multi-sensor fusion for underwater vehicle localization by augmentation of RBF neural network and error-state Kalman filter. Sensors, 21(4), 1149. https://doi.org/10.3390/s21041149

[30] Markovic, I., Kovac, M., & Milijas, R. (2022). Error state extended Kalman filter multi-sensor fusion for unmanned aerial vehicle localization in GPS and magnetometer denied indoor environments. 2022 International Conference on Unmanned Aircraft Systems. https://doi.org/10.1109/icuas54217.2022.9836124

[31] Katwe, M., Iyer, S., & Khan, M. (2021). Particle filter-based localization of autonomous vehicle. 2021 2nd Global Conference for Advancement in Technology. https://doi.org/10.1109/gcat52182.2021.9587461

[32] Kaygusuz, B., Mendez, O., & Bowden, R. (2021). Multi-camera sensor fusion for visual odometry using deep uncertainty estimation. 2021 IEEE International Intelligent Transportation Systems Conference. https://doi.org/10.1109/itsc48978.2021.9565079

[33] Zhang, K., Khoshelham, K., & Khodabandeh, A. (2021). Seamless vehicle positioning by Lidar-GNSS integration: Standalone and multi-epoch scenarios. Remote Sensing, 13(22), 4525. https://doi.org/10.3390/rs13224525

[34] Farag, W. (2020). Road-objects tracking for autonomous driving using lidar and radar fusion. Journal of Electrical Engineering, 71(3), 138-149. https://doi.org/10.2478/jee-2020-0021

[35] Jing, Y., Han, J., Ding, W., & Wang, X. (2022). Intrinsic and extrinsic calibration of roadside LiDAR and camera. 2022 China Automation Congress. https://doi.org/10.1109/cac57257.2022.10054792

[36] Martins, P., Costelha, H., & Bento, C. (2020). Monocular camera calibration for autonomous driving: A comparative study. 2020 IEEE ICARSC. https://doi.org/10.1109/icarsc49921.2020.9096104

[37] Zhang, J., & Xu, Y. (2022). Extrinsic calibration of LiDAR-camera based on deep convolutional network. 2022 China Automation Congress. https://doi.org/10.1109/cac57257.2022.10055799

[38] Lee, J., & Johnson, E. N. (2020). Latency compensated visual-inertial odometry for agile autonomous flight. Sensors, 20(8), 2209. https://doi.org/10.3390/s20082209

[39] Chen, C., Pu, H., & Chen, R. (2022). WHUVID: A large-scale stereo-IMU dataset for visual-inertial odometry and autonomous driving in Chinese urban scenarios. Remote Sensing, 14(9), 2033. https://doi.org/10.3390/rs14092033

[40] Li, Z., Zhao, J., & Kang, Y. (2019). DL-SLAM: Direct 2.5D LiDAR SLAM for autonomous driving. 2019 IEEE Intelligent Vehicles Symposium. https://doi.org/10.1109/ivs.2019.8813868